Available online at www.sciencedirect.com
SCIENCE DIRECT®
Journal of Sound and Vibration 270 (2004) 75–92
JOURNAL OF SOUND AND VIBRATION
www.elsevier.com/locate/jsvi

Triple resonant states and chaos control in an electrostatic transducer with two outputs

Y. Chembo Kouomou[a,b], P. Woafo[a,*]

[a] *Laboratoire de Mécanique, Faculté des Sciences, Université de Yaoundé I, B.P. 812, Yaoundé, Cameroon*
[b] *Division of Telecommunication Technical Studies, Minpostel, Yaoundé, Cameroon*

Received 17 July 2002; accepted 12 December 2002

Abstract

The dynamics of a non-linear electrostatic transducer with two outputs is studied. The amplitudes and stability conditions of oscillations for the Triple Resonant States are obtained and discussed. It is found that chaos can appear in the system. A retroactive control strategy is therefore applied to tune these chaotic oscillations to regular target orbits. The stability analysis of the feedback controller is also investigated, and an estimation of the feedback strength under which no efficient control is possible is derived. The analytic study is confirmed by numerical simulations.

1. Introduction

Research in the area of coupled non-linear oscillators has received a great deal of attention in recent years. This is due to the fact that coupled oscillators provide fundamental models for the dynamics of various physical, electrical, mechanical and biological systems (see Refs. [1–5] and references therein).

In the field of electromechanical systems, recent studies have highlighted that even though they are undesirable and harmful most of the time [6], non-linear phenomena could find valuable applications in some particular cases [7]. It is in this spirit that a non-linear electrostatic transducer with two outputs is studied in this paper. This electromechanical system can serve as a multi-frequency industrial or domestic shaker. Its principal advantages are a conceptual simplicity, an easy implementation and a remarkable robustness. The analysis of this system will show that owing to non-linearity, a common uniperiodic electric excitation (for example the

*Corresponding author.
E-mail address: pwoafo@uycdc.uninet.cm (P. Woafo).

0022-460X/03/$ - see front matter
doi:10.1016/S0022-460X(03)00484-X

voltage of the mains) can provide several sets of amplitudes and frequencies for the two mechanical outputs.

Depending on the numerical values of the non-linearity and coupling parameters, the electrostatic transducer can display a chaotic behaviour, which may be a positive or a negative tool depending on the precise utilization [8,9]. The consequent aim is to design a feedback controller able to tune the chaotic trajectories to suitable target orbits if necessary. The stability of the control process, which is currently an opened question, will be particularly investigated as well as the determination of the critical control parameters leading to a satisfying control.

The paper is organized as follows. In Section 2, the electromechanical system and its equations of motion are presented. The equilibrium points are exhaustively identified, and their stability analysis is performed. Using the Multiple Time Scales Method the three triple resonant states (TRS) of the model are analyzed in Section 3. A direct numerical simulation of the evolution equation shows an excellent agreement with the analytical amplitudes of these TRS. The stability analysis of these resonant states is also discussed. Section 4 deals with the chaotic behaviour of the transducer and the control of the system from chaos to regular target orbits. Various considerations about the suitable characteristics of the controller will be particularly investigated. Conclusions are given in Section 5. The numerical simulation of all ordinary differential equations will be carried out with the fourth order Runge–Kutta algorithm, while all the non-linear algebraic equations will be solved through the Newton–Raphson algorithm.

2. The electromechanical system

2.1. Equations of motion

The electrostatic transducer with two outputs is schematically represented in Fig. 1. It consists of a resistive part (R_0, R_1 and R_2), an inductive component (L_0), and a capacitive part (C_0, C_1 and

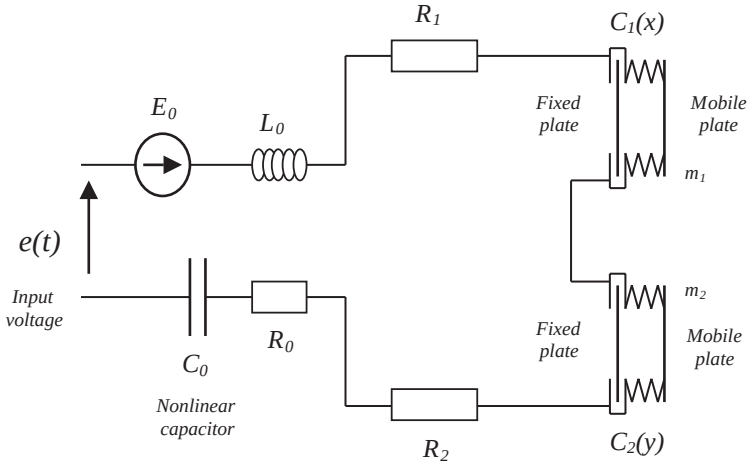

Fig. 1. Schematic representation of the non-linear electrostatic transducer with two outputs.

C_2) which is polarized by a high-voltage accumulator E_0. C_1 and C_2 are plane capacitors with a fixed and a mobile plate each, while C_0 is a non-linear capacitor (of a semiconductor type) with a Duffing-like charge–voltage characteristic. The system is excited by a sinusoidal external voltage $e(t)$ which thereby induces the vibration of the mobile plates of C_1 and C_2. The masses of these mobile plates are respectively equal to m_1 and m_2.

The Lagrangian and the dissipation function corresponding to the electromechanical system can respectively be expressed as

$$\begin{aligned} \Lambda = &\left(\tfrac{1}{2}m_1\dot{x}^2 + \tfrac{1}{2}m_2\dot{y}^2 + \tfrac{1}{2}L_0\dot{q}^2\right) \\ &- \left(\tfrac{1}{2}k_1(d_1+x)^2 + \tfrac{1}{2}k_2(d_2+y)^2 + \frac{(Q_0+q)^2}{2C_{eq}(x,y)} + \frac{1}{4}\chi q^4\right) \\ &+ (Q_0+q)(E_0 + e_0\cos(\Omega t)) \end{aligned} \tag{1a}$$

and

$$D = \tfrac{1}{2}\eta_1\dot{x}^2 + \tfrac{1}{2}\eta_2\dot{y}^2 + \tfrac{1}{2}(R_0+R_1+R_2)\dot{q}^2, \tag{1b}$$

where

$$C_{eq}(x,y) = \left(\frac{1}{C_0} + \frac{(1-x/d_1)}{C_1} + \frac{(1-y/d_2)}{C_2}\right)^{-1} \tag{2}$$

is the instantaneous equivalent capacitance of the electrical circuit. Here, x and y are the displacements of the mobile plates of C_1 and C_2, while q is the instantaneous electric charge in the electrical loop. η_1 and η_2 are the mechanical dissipative coefficients, d_1 and d_2 represent the distance between the plates of the two plane capacitors, and χ is the Duffing coefficient. $C_{eq}(0,0) = C_{eq} = (1/C_0 + 1/C_1 + 1/C_2)^{-1}$ is the equivalent capacitor of the circuit at the trivial equilibrium, and $Q_0 = C_{eq}E_0$ is the polarization static electric charge.

Taking into account the polarization conditions, the equations of motion can be expressed as

$$\begin{aligned} &m_1\ddot{x} + \eta_1\dot{x} + k_1 x - \frac{Q_0}{C_1 d_1}q - \frac{1}{2C_1 d_1}q^2 = 0, \\ &m_2\ddot{y} + \eta_2\dot{y} + k_2 y - \frac{Q_0}{C_2 d_2}q - \frac{1}{2C_2 d_2}q^2 = 0, \\ &L_0\ddot{q} + (R_0+R_1+R_2)\dot{q} + \frac{q}{C_{eq}} + \chi q^3 - \left(\frac{1}{C_1 d_1}x + \frac{1}{C_2 d_2}y\right)(Q_0+q) = e_0\cos(\Omega t). \end{aligned} \tag{3}$$

After a suitable normalization, the equations of motion (3) can be rewritten as

$$\begin{aligned} &\ddot{x} + \lambda_{10}\dot{x} + \omega_1^2\left(x - \alpha_{10}\left(q + \tfrac{1}{2}q^2\right)\right) = 0, \\ &\ddot{y} + \lambda_{20}\dot{y} + \omega_2^2\left(y - \alpha_{20}\left(q + \tfrac{1}{2}q^2\right)\right) = 0, \\ &\ddot{q} + \lambda_{e0}\dot{q} + q + \gamma_0 q^3 - (\mu_{10}x + \mu_{20}y)(1+q) = U_{m0}\cos\omega t. \end{aligned} \tag{4}$$

In Eq. (4), x and y have been expressed relatively to $d = \sqrt{d_1 d_2}$, q relatively to Q_0 and t relatively to $\Omega_e^{-1} = \sqrt{L_0 C_{eq}}$. The new dimensionless parameters are related to the

true ones by

$$\lambda_{n0} = \frac{\eta_n}{m_n \Omega_e}, \quad \omega_n = \sqrt{\frac{k_n/m_n}{1/L_0 C_{eq}}}, \quad \alpha_{n0} = \frac{Q_0^2/2C_n}{k_n d_n^2/2}\frac{d}{d_n}, \quad \mu_{n0} = \frac{C_{eq}}{C_n}\frac{d}{d_n} \quad \text{with } n = 1 \text{ or } 2,$$
$$\lambda_{e0} = \frac{(R_0 + R_1 + R_2)}{L_0 \Omega_e}, \quad \gamma_0 = \frac{\chi Q_0^2}{L_0 \Omega_e^2}, \quad \omega = \frac{\Omega}{\Omega_e}, \quad U_{m0} = \frac{e_0}{L_0 Q_0 \Omega_e^2}. \tag{5}$$

The transducer is now described by several dimensionless parameters. λ_{e0}, λ_{10} and λ_{20} are damping coefficients, while ω_1 and ω_2 are kinematic coefficients proportional to the natural frequencies of the mobile plates. The coupling of the mechanical parts to the electrical one is ensured by the energetic coefficients α_{10} and α_{20}, which define the ratio between equilibrium electrostatic and mechanical energies. The variable q is in its turn non-linearly coupled to x and y through the geometrical coefficients μ_{10} and μ_{20} which depend on the shape and dimensions of the transducer. At last, the Duffing non-linearity is recovered through the coefficient γ_0. The utilization of a Duffing-like non-linear capacitor has been considered to enable the hysteresis phenomenon to appear. Effectively, it is known that this critical phenomenon can serve for the switching between the two different amplitudes corresponding to the higher and lower nearby frequencies situated just around the jumping frequency. In that case, slight deviations of the external forcing frequency would be sufficient to command different functioning modes of the transducer's dynamics with a reduced energy consumption.

2.2. Equilibrium states and their stability

Eqs. (4) can be rewritten under the vectorial form

$$\dot{\mathbf{u}} = \mathbf{F}(\mathbf{u}) + \mathbf{E}(t), \tag{6a}$$

where $\mathbf{u} = (x, \dot{x}, y, \dot{y}, q, \dot{q})$ is the six-dimensional state vector. The non-linear flow $\mathbf{F}$ represents the motion equations of the non-excited transducer and $\mathbf{E}$ the external excitation. The equilibrium states $\mathbf{u_{eq}}$ are solutions of the set of non-linear algebraic equations $\mathbf{F}(\mathbf{u_{eq}}) = \mathbf{0}$. Since x_{eq} and y_{eq} are univocally bound to q_{eq}, the equilibrium states can be exhaustively determined through the resolution of the following polynomial equation:

$$q_{eq}\left[\left(\gamma_0 - \tfrac{1}{2}\beta_{12}\right)q_{eq}^2 + \left(-\tfrac{3}{2}\beta_{12}\right)q_{eq} + (1 - \beta_{12})\right] = 0 \tag{6b}$$

with $\beta_{12} = \mu_{10}\alpha_{10} + \mu_{20}\alpha_{20}$. It straightforwardly appears that the trivial centre point is always an equilibrium state of the system ($q_{eq} = 0$). Depending on the different parameters of the transducer, a variable number of asymmetric equilibrium states can also coexist. More precisely, if the critical value is defined as

$$\gamma_{0,cr} = \frac{\beta_{12}^2 + 8\beta_{12}}{16(1 - \beta_{12})} \tag{6c}$$

it can be demonstrated that there is one asymmetric fixed point when $\gamma_0 \in \{(\beta_{12}/2),\ \gamma_{0,cr}\}$ or $\beta_{12} = 1$, two when $\gamma_0 < \gamma_{0,cr}$, but none for $\gamma_0 = \beta_{12}/2 = 1/2$ or $\gamma_0 > \gamma_{0,cr}$.

The local stability analysis of these equilibrium states can be determined by investigating the linearized system

$$\delta\dot{\mathbf{u}} = \left[\frac{\partial \mathbf{F}}{\partial \mathbf{u}}\right] \cdot \delta\mathbf{u} \quad \text{at } \mathbf{u} = \mathbf{u_{eq}}. \tag{6d}$$

The perturbation $\delta\mathbf{u}$ asymptotically decays to zero if the sixth order Jacobian matrix $[\partial\mathbf{F}/\partial\mathbf{u}]$ has strictly negative eigenvalues. The Routh–Hurwitz criterion and the physical constraints inherent to the electromechanical system guarantee that it is the case provided that

$$\left(\gamma_0 - \tfrac{1}{2}\right) q_{eq}^2 - \beta_{12} q_{eq} + \tfrac{1}{3}(1 - \beta_{12}) > 0. \tag{6e}$$

Therefore, a given equilibrium state can be stable if and only if it fulfills the stability constraint (6e). It can be consequently deduced that for example, the trivial centre point is asymptotically stable when $\beta_{12} < 1$.

3. The triple resonant states

3.1. The multiple time scales method

Amongst all the analytic approaches for the non-linear oscillations, the multiple time scales method (MTSM) has been chosen because it is the most adapted to the study of dynamical systems around resonance frequencies [1,4,5,8,9]. In this paper, the damping, the coupling, the external excitation and the non-linearity are considered as global first order perturbations. Therefore write $U_{m0} = \varepsilon U_0$, $\lambda_{e0} = \varepsilon\lambda_e, \gamma_0 = \varepsilon\gamma$, and $\lambda_{k0} = \varepsilon\lambda_k, \alpha_{k0} = \varepsilon\alpha_k, \mu_{k0} = \varepsilon\mu_k$ $(k = 1, 2)$, ε being a scale factor.

One is therefore led to seek a first order asymptotic expansion in the form

$$\begin{aligned} x &= x_0(T_0, T_1) + \varepsilon x_1(T_0, T_1) + O(\varepsilon^2), \\ y &= y_0(T_0, T_1) + \varepsilon y_1(T_0, T_1) + O(\varepsilon^2), \\ q &= q_0(T_0, T_1) + \varepsilon q_1(T_0, T_1) + O(\varepsilon^2). \end{aligned} \tag{7}$$

The independent time scales $T_0 = t$ and $T_1 = \varepsilon t$ are respectively the fast scale (associated to the unperturbed system) and the slow scale (associated to the amplitude and phase modulations induced by the global first order perturbation). Substituting Eqs. (7) into Eqs. (4) and equating coefficients of like powers of ε, one obtains the following set of ordinary differential equations:

Order ε^0

$$\begin{aligned} D_0^2 x_0 + \omega_1^2 x_0 &= 0, \\ D_0^2 y_0 + \omega_2^2 y_0 &= 0, \\ D_0^2 q_0 + q_0 &= 0. \end{aligned} \tag{8}$$

Order ε^1

$$
\begin{aligned}
&D_0^2 x_1 + \omega_1^2 x_1 = \alpha_1 \omega_1^2 \left(q_0 + \tfrac{1}{2} q_0^2\right) - 2D_0 D_1 x_0 - \lambda_1 D_0 x_0,\\
&D_0^2 y_1 + \omega_2^2 y_1 = \alpha_2 \omega_2^2 \left(q_0 + \tfrac{1}{2} q_0^2\right) - 2D_0 D_1 y_0 - \lambda_2 D_0 y_0,\\
&D_0^2 q_1 + q_1 = (\mu_1 x_0 + \mu_2 y_0)(1 + q_0) - 2D_0 D_1 q_0 - \lambda_e D_0 q_0 - \gamma q_0^3 + U_0 \cos \omega t
\end{aligned} \tag{9}
$$

with $D_n = \partial/\partial T_n$, $n = 0, 1$. The general solution of Eqs. (8) can be expressed as

$$
\begin{aligned}
x_0 &= A(T_1) \exp(\mathrm{j}\omega_1 T_0) + \bar{A}(T_1) \exp(-\mathrm{j}\omega_1 T_0),\\
y_0 &= B(T_1) \exp(\mathrm{j}\omega_2 T_0) + \bar{B}(T_1) \exp(-\mathrm{j}\omega_2 T_0),\\
q_0 &= C(T_1) \exp(\mathrm{j} T_0) + \bar{C}(T_1) \exp(-\mathrm{j} T_0),
\end{aligned} \tag{10}
$$

where the overbar represents the complex conjugate and $\mathrm{j}^2 = -1$. One should notice that A, B and C are undetermined functions at this point, but will be determined by imposing solvability conditions in the next approximation equations. Therefore, substituting x_0, y_0 and q_0 into Eqs. (9) yields

$$
\begin{aligned}
D_0^2 x_1 + \omega_1^2 x_1 =& \tfrac{1}{2} \alpha_1 \omega_1^2 C \bar{C} + \tfrac{1}{2} \alpha_1 \omega_1^2 C^2 \exp(2\mathrm{j} T_0) + \alpha_1 \omega_1^2 C \exp(\mathrm{j} T_0)\\
&- \mathrm{j}\omega_1 (2A' + \lambda_1 A) \exp(\mathrm{j}\omega_1 T_0) + \text{Comp. Conj.},
\end{aligned}
$$

$$
\begin{aligned}
D_0^2 y_1 + \omega_2^2 y_1 =& \tfrac{1}{2} \alpha_2 \omega_2^2 C \bar{C} + \tfrac{1}{2} \alpha_2 \omega_2^2 C^2 \exp(2\mathrm{j} T_0) + \alpha_2 \omega_2^2 C \exp(\mathrm{j} T_0)\\
&- \mathrm{j}\omega_2 (2B' + \lambda_2 B) \exp(\mathrm{j}\omega_2 T_0) + \text{Comp. Conj.},
\end{aligned}
$$

$$
\begin{aligned}
D_0^2 q_1 + q_1 =& + \mu_1 (A \exp(\mathrm{j}\omega_1 T_0) + AC \exp(\mathrm{j}(\omega_1 + 1) T_0) + A\bar{C} \exp(\mathrm{j}(\omega_1 - 1) T_0))\\
&+ \mu_2 (B \exp(\mathrm{j}\omega_2 T_0) + BC \exp(\mathrm{j}(\omega_2 + 1) T_0) + B\bar{C} \exp(\mathrm{j}(\omega_2 - 1) T_0))\\
&- (2\mathrm{j}C' + \mathrm{j}\lambda_e C + 3\gamma C^2 \bar{C}) \exp(\mathrm{j} T_0) - \gamma C^3 \exp(3\mathrm{j} T_0)\\
&+ \tfrac{1}{2} U_0 \exp(\mathrm{j}\omega T_0) + \text{Comp.Conj.}
\end{aligned} \tag{11}
$$

The prime here (over A, B and C) and throughout all the paper indicates the differentiation with respect to T_1, and "Comp. Conj." will stand for the complex conjugate of all the preceding terms.

As was observed earlier, the unknown amplitudes A, B and C may now be determined by eliminating secular terms in Eqs. (11). However, because of the high dimensionality of the system, it is impossible to obtain unambiguously a set of secular equations valid for all frequencies. One is therefore compelled to distinguish different cases of harmonic resonance (according to the different values of the frequencies ω_1, ω_2 and ω relatively to the electric natural frequency $\omega_e = 1$) which are leading to different sets of secular equations. Various types of resonant states can be found from Eqs. (11). But in this paper, the emphasis is placed on TRS. In fact, the other resonant states are not particularly interesting since they lead to the states of no motion for one or two of the three oscillators. Along the same line, sub- and super-harmonic resonances have not been considered here firstly because some of them cannot be straightforwardly deduced from the MTSM, and secondly because they do not generally induce noticeable amplitudes. Owing to the structural symmetry of the two mechanical oscillators equations of motion, this multitude of TRS can mathematically be reduced to three, that is $\omega_1 = \omega_2 = \omega = \omega_e$ (first TRS), $\omega_1 = \omega_2 = 2\omega = 2\omega_e$ (second TRS), and at last $2\omega_1 = \omega_2 = 2\omega = 2\omega_e$ (third TRS). The study of these TRS obviously includes those of double resonant states and simple resonant states. Hence, one can

consider that all the possible resonances of the non-linear transducer are here exhaustively explored.

3.2. Amplitude of non-linear oscillations in the TRS

For the illustration of the analytic procedure, consider the first TRS where the external excitation frequency is approximately equal to the natural frequencies of the electric and mechanical oscillators. Then set

$$\omega = 1 + \varepsilon\xi, \quad \omega_1 = 1 + \varepsilon\xi_1, \quad \omega_2 = 1 + \varepsilon\xi_2, \tag{12}$$

where ξ_1, ξ_2 and ξ are detuning parameters expressing the quantitative nearness of the resonance frequencies ω_1, ω_2 and ω with the fixed electric natural frequency $\omega_e = 1$. Hence, inserting Eqs. (12) into Eq. (11) leads to the following solvability conditions:

$$\begin{aligned}
&\alpha_1\omega_1^2 C\exp(-\mathrm{j}\xi_1 T_1) - \mathrm{j}\omega_1(2A' + \lambda_1 A) = 0,\\
&\alpha_2\omega_2^2 C\exp(-\mathrm{j}\xi_2 T_1) - \mathrm{j}\omega_2(2B' + \lambda_2 B) = 0,\\
&\mu_1 A\exp(\mathrm{j}\xi_1 T_1) + \mu_2 B\exp(\mathrm{j}\xi_2 T_1) - (2\mathrm{j}C' + \mathrm{j}\lambda_e C + 3\gamma C^2\bar{C}) + \tfrac{1}{2}U_0\exp(\mathrm{j}\xi T_1) = 0.
\end{aligned} \tag{13}$$

Expressing $A(T_1), B(T_1), C(T_1)$ in the polar form yields

$$\begin{aligned}
A(T_1) &= \tfrac{1}{2}a_1(T_1)\exp(\mathrm{j}b_1(T_1)),\\
B(T_1) &= \tfrac{1}{2}a_2(T_1)\exp(\mathrm{j}b_2(T_1)),\\
C(T_1) &= \tfrac{1}{2}a_3(T_1)\exp(\mathrm{j}b_3(T_1)),
\end{aligned} \tag{14}$$

where a_k and b_k are respectively the amplitudes and the phases of the oscillators. After separating the real and imaginary parts in Eqs. (13), one obtains the following set of first order ordinary differential equations:

$$\begin{aligned}
&\tfrac{1}{2}\alpha_1\omega_1 a_3\cos\psi_1 + a_1 b_1' = 0,\\
&\tfrac{1}{2}\alpha_1\omega_1 a_3\sin\psi_1 + \left(a_1' + \tfrac{1}{2}\lambda_1 a_1\right) = 0,\\
&\tfrac{1}{2}\alpha_2\omega_2 a_3\cos\psi_2 + a_2 b_2' = 0,\\
&\tfrac{1}{2}\alpha_2\omega_2 a_3\sin\psi_2 + \left(a_2' + \tfrac{1}{2}\lambda_2 a_2\right) = 0,\\
&a_3 b_3' - \tfrac{3}{8}\gamma a_3^3 + \tfrac{1}{2}U_0\cos\psi_3 + \tfrac{1}{2}\mu_1 a_1\cos\psi_1 + \tfrac{1}{2}\mu_2 a_2\cos\psi_2 = 0,\\
&a_3' + \tfrac{1}{2}\lambda_e a_3 - \tfrac{1}{2}U_0\sin\psi_3 - \tfrac{1}{2}\mu_1 a_1\sin\psi_1 - \tfrac{1}{2}\mu_2 a_2\sin\psi_2 = 0,
\end{aligned} \tag{15}$$

where $\psi_1 = \xi_1 T_1 + b_1 - b_3$, $\psi_2 = \xi_2 T_1 + b_2 - b_3$ and $\psi_3 = \xi T_1 - b_3$. Since one is particularly interested in studying the steady state responses, first impose $(a_1' = 0; a_2' = 0; a_3' = 0)$ and secondly $(\psi_1' = 0; \psi_2' = 0; \psi_3' = 0)$, which implies $(b_1' = \xi - \xi_1;\ b_2' = \xi - \xi_2; b_3' = \xi)$. Thus eliminating ψ_1, ψ_2 and ψ_3 from Eqs. (15), one can obtain the following resonance equation:

$$\tfrac{9}{64}\gamma^2 a_3^6 + \tfrac{3}{4}\gamma(M_{11} + M_{21} - \xi)a_3^4 + \left[(M_{11} + M_{21} - \xi)^2 + \left(\tfrac{1}{2}\lambda_e + N_{11} + N_{21}\right)^2\right]a_3^2 - \tfrac{1}{4}U_0^2 = 0 \tag{16}$$

and the following coupling relations:

$$\begin{aligned}
a_1 &= \tfrac{1}{2}\alpha_1\omega_1 G_{11} a_3,\\
a_2 &= \tfrac{1}{2}\alpha_2\omega_2 G_{21} a_3
\end{aligned} \tag{17}$$

with

$$G_{ik} = \left[(\xi_i - k\xi)^2 + \tfrac{1}{4}\lambda_i^2\right]^{-1/2},$$
$$M_{ik} = \tfrac{1}{4}\mu_i\alpha_i\omega_i(k\xi - \xi_i)G_{ik}^2, \quad i \text{ and } k = 1, 2.$$
$$N_{ik} = \tfrac{1}{8}\mu_i\alpha_i\omega_i\lambda_i G_{ik}^2, \tag{18}$$

The mechanical amplitudes are here directly proportional to a_3.

For the second TRS, the natural frequencies of the two mechanical oscillators are nearly double those of the electrical and external frequencies, so that

$$\omega = 1 + \varepsilon\xi, \quad \omega_1 = 2 + \varepsilon\xi_1, \quad \omega_2 = 2 + \varepsilon\xi_2. \tag{19}$$

Using the same procedure as above for the first TRS, one obtains the following resonance equation

$$\tfrac{1}{64}[(3\gamma + M_{12} + M_{22})^2 + (N_{12} + N_{22})^2]a_3^6 + \tfrac{1}{8}[\lambda_e(N_{12} + N_{22}) - 2\xi(3\gamma + M_{12} + M_{22})]a_3^4 + \left(\xi^2 + \tfrac{1}{4}\lambda_e^2\right)a_3^2 - \tfrac{1}{4}U_0^2 = 0 \tag{20}$$

with

$$a_1 = \tfrac{1}{8}\alpha_1\omega_1 G_{12}a_3^2,$$
$$a_2 = \tfrac{1}{8}\alpha_2\omega_2 G_{22}a_3^2. \tag{21}$$

Here, the amplitudes of a_1 and a_2 are proportional to the square of a_3 rather than a_3 itself like in the first TRS.

The third and last TRS corresponds to the situation where

$$\omega = 1 + \varepsilon\xi, \quad \omega_1 = 1 + \varepsilon\xi_1, \quad \omega_2 = 2 + \varepsilon\xi_2. \tag{22}$$

The vibration frequency of the second mechanical oscillator is twice that of the first one. The resonance equation is therefore

$$\tfrac{1}{64}[(3\gamma + M_{22})^2 + N_{22}^2]a_3^6 + \tfrac{1}{4}\left[(3\gamma + M_{22})(M_{11} - \xi) + N_{22}\left(\tfrac{1}{2}\lambda_e + N_{11}\right)\right]a_3^4 + \left[(M_{11} - \xi)^2 + \left(\tfrac{1}{2}\lambda_e + N_{11}\right)^2\right]a_3^2 - \tfrac{1}{4}U_0^2 = 0 \tag{23}$$

with

$$a_1 = \tfrac{1}{2}\alpha_1\omega_1 G_{11}a_3,$$
$$a_2 = \tfrac{1}{8}\alpha_2\omega_2 G_{22}a_3^2. \tag{24}$$

In this latter case, one mechanical amplitude is proportional to a_3 while the other is proportional to the square of a_3.

Using the Newton–Raphson algorithm, the amplitudes a_1, a_2 and a_3 are plotted as functions of the detuning parameter ξ ($\xi_1 = \xi_2 = 0$ will be consider throughout all the paper). As ξ is increased, the hysteresis phenomenon appears and some observations can be made. For instance, since the initial condition is the trivial centre point, one can notice in Figs. 2–4 that for each amplitude, the results of the direct numerical simulation of Eqs. (4) only agree with the lowest

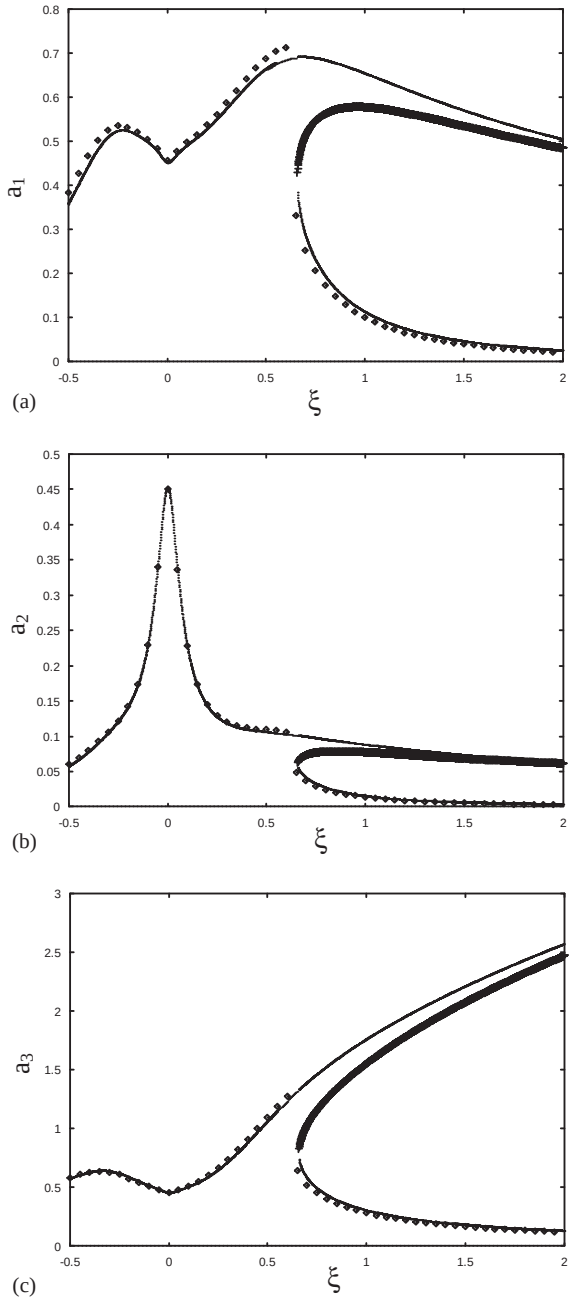

Fig. 2. First TRS, with $\alpha_1 = 0.8,\ \alpha_2 = 0.1,\ \mu_1 = 0.9,\ \mu_2 = 0.1,\ \lambda_1 = 0.8,\ \lambda_2 = 0.1,\ \lambda_e = 0.1,\ \gamma = 0.8,\ U_0 = 0.5$ and $\varepsilon = 0.1$. (a) Frequency–response curve for a_1, with analytical results in thin or thick lines, and numerical results in squares; (b) idem for a_2; (c) idem for a_3.

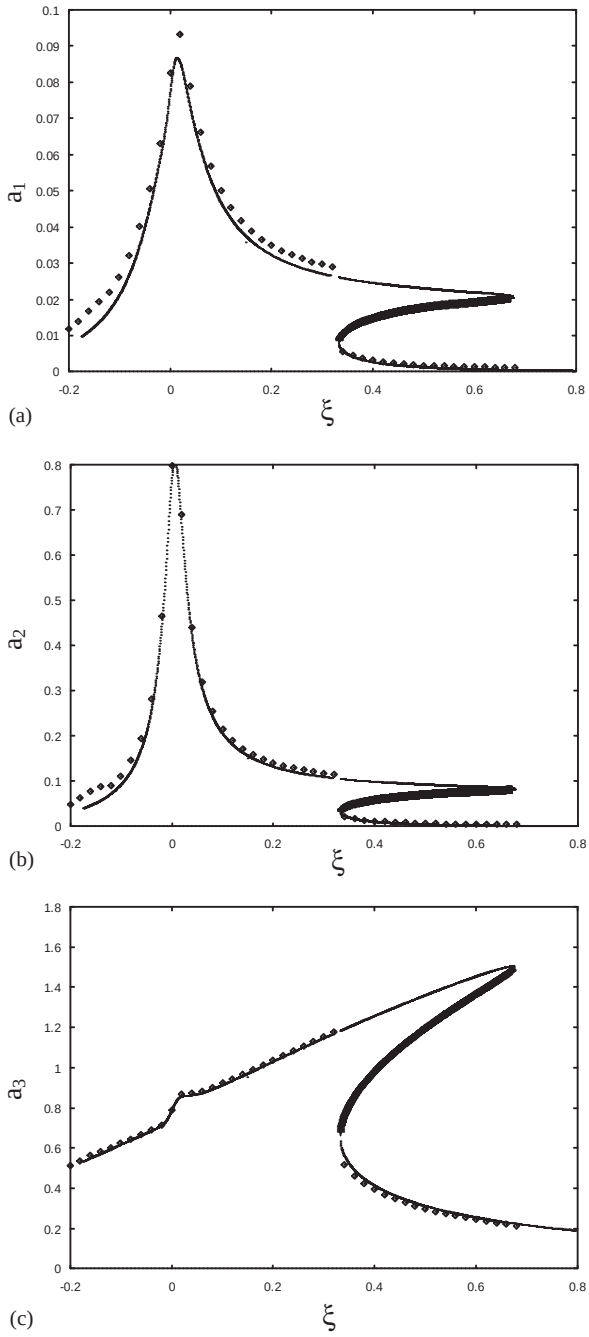

Fig. 3. Second TRS, with $\alpha_1 = 0.05,\ \alpha_2 = 0.2,\ \mu_1 = 0.2,\ \mu_2 = 0.3,\ \lambda_1 = 0.2,\ \lambda_2 = 0.08,\ \lambda_e = 0.2,\ \gamma = 0.8,\ U_0 = 0.3$ and $\varepsilon = 0.1$. (a) Frequency–response curve for a_1, with analytical results in thin or thick lines, and numerical results in squares; (b) idem for a_2; (c) idem for a_3.

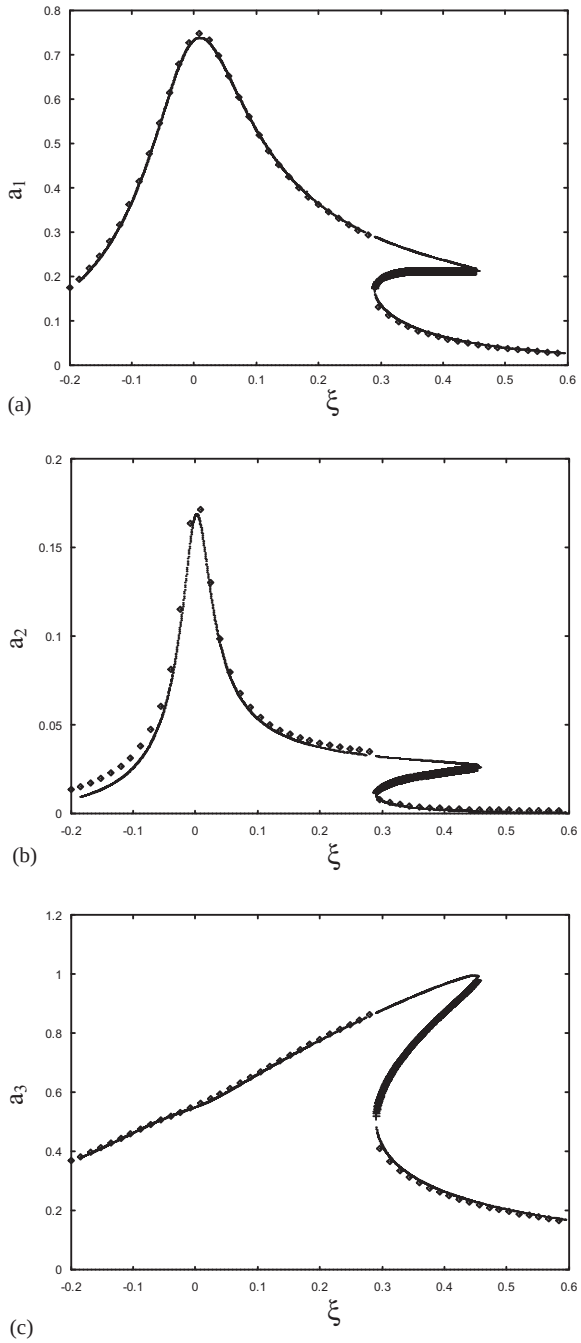

Fig. 4. Third TRS, with $\alpha_1 = 0.2$, $\alpha_2 = 0.1$, $\mu_1 = 0.03$, $\mu_2 = 0.1$, $\lambda_1 = 0.15$, $\lambda_2 = 0.09$, $\lambda_e = 0.2$, $\gamma = 1.2$, $U_0 = 0.2$ and $\varepsilon = 0.1$. (a) Frequency–response curve for a_1, with analytical results in thin or thick lines, and numerical results in squares; (b) idem for a_2; (c) idem for a_3.

branch. Hence, the transition from the single valued to the multivalued areas enables the jump phenomenon to appear. This has yet been observed during the analogue simulation of the regular dynamics of coupled non-linear oscillators [10]. It is also interesting to notice on these figures the accuracy of the analytic treatment which has been performed. It confirms that the transducer should preferably work at resonance amplitudes because of the highest mechanical amplitudes.

3.3. Stability of oscillations in the TRS

The problem of dynamic stability is bound with the inherent non-linearity of the system. To determine the stability of the oscillatory states which have yet to be obtained, they are perturbed and the asymptotic behaviour of the related perturbations δa_k and $\delta\psi_k$ are studied as the time tends to infinity. It is found that the perturbation for each TRS case is governed by a linear sixth-dimensional flow, so that the stability of an oscillatory state is thereby reduced to the stability of the related perturbation flow. Consequently, for each TRS and for a given oscillatory state $(\delta a_k, \delta\psi_k)$, the steady state motion will be stable if all the eigenvalues of the perturbation matrix have negative real parts. Because of the high dimensionality of this matrix, the analytic determination of these eigenvalues leads to quite large analytical expressions. That is why a numerical algorithm has been used to compute these eigenvalues, and the results are also in Figs. 2, 3 and 4 where the stable points constitute a thin line, and unstable points a thick line. One can hence observe that for the chosen system parameters, instability only appears for the second branch of the hysteresis area, and never in the single-valued area as it can be the case for other three-degree-of-freedom systems [5].

4. Chaotic behaviour and canonical feedback control

Depending on the set of chosen parameters, the system can display chaotic dynamics, as can be seen in the bifurcation diagram of Fig. 5. On the one hand, it has appeared in recent years that chaos can be converted to a positive tool due particularly to the flexibility of systems motion in chaotic states, and to the infinite number of trajectories embedded in a chaotic attractor. For instance, chaos in an electrostatic transducer can be used to encrypt or secure audio-messages in communication engineering [11]. On the other hand, chaos can induce undesirable consequences such as early fatigue failures in electromechanical systems [7,9,12–14].

One therefore needs to tune the electromechanical transducer to a regular target orbit for the performance requirements to be fulfilled. The next subsections will particularly investigate the conditions under which a convenient control can be achieved.

4.1. Target orbits and stability of the control

The aim of this section is to use the canonical feedback control scheme to tune the chaotic state vector $\mathbf{u}$ to the target state $\bar{\mathbf{u}}$, so that

$$\lim_{t\to+\infty} ||\mathbf{u}(t) - \bar{\mathbf{u}}(t)|| < h, \tag{25}$$

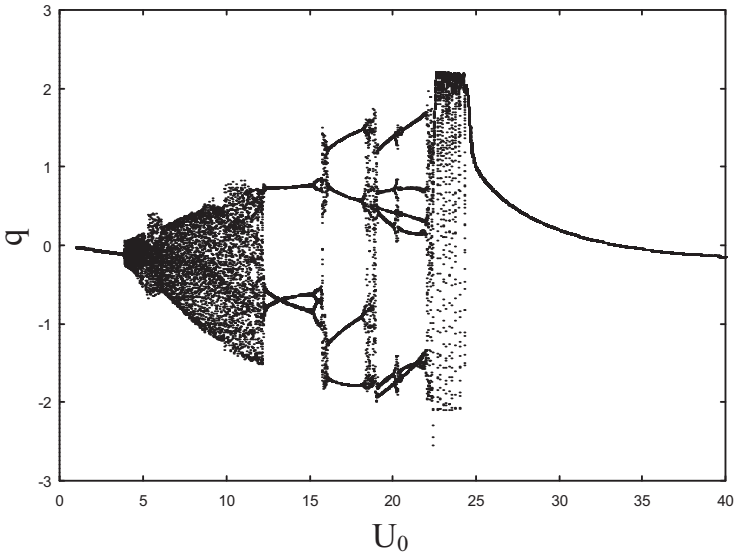

Fig. 5. Bifurcation diagram (U_0, q) showing the transitions to chaos, with $\alpha_1 = 0.8$, $\alpha_2 = 0.9$, $\mu_1 = 2.0$, $\mu_2 = 1.5$, $\omega_1 = 1.0$, $\omega_2 = 1.0$, $\lambda_1 = 0.1$, $\lambda_2 = 0.1$, $\lambda_e = 0.1$, $\omega = 1.0$, $\gamma = 8.0$, and $\varepsilon = 0.1$.

where h is the precision of the control. The conventional feedback theory approach leads to the following control equation

$$\dot{\mathbf{u}} = \{\mathbf{F}(\mathbf{u}) + \mathbf{E}(t)\} - [\mathbf{K}](\mathbf{u} - \bar{\mathbf{u}}) = \mathbf{F}^{(\mathbf{c})}(\mathbf{u}, \bar{\mathbf{u}}, t), \tag{26}$$

where $[\mathbf{K}]$ is (6×6) feedback gain matrix, and $\mathbf{F}^{(\mathbf{c})}(\mathbf{u}, \bar{\mathbf{u}}, t)$ a new six-dimensional vector-flow. In view of practical applications, set $K_{ij} \equiv 0$ except $K_{65} \equiv K$, i.e., the control is ensured with only one coefficient over 36. Physically, this control scheme corresponds to the connection of a control current-source in parallel with the capacitive component of the electrical circuit. Therefore, K controls q to $\bar{q}$, so that x and y are automatically tuned to their related $\bar{x}$ and $\bar{y}$ target values according to Eqs. (4). Note that one can also relate the controller directly to the mechanical oscillators.

It can be demonstrated that chaos control is optimized when the target orbit is the nearest possible to an unstable periodic orbit (UPO) embedded within the chaotic attractor [15]. Moreover, we have noticed during the numerical simulations that even though the lowest and the highest branches of the hysteresis area are both theoretically stable (Figs. 2–4), the lowest branch is always more easily reached than the highest, whatever the initial conditions are. Since the highest amplitudes are preferably required for the optimal functioning regime of an electromechanical system, consider as target orbit the upper branch of the hysteresis curve. Consequently, take as the target orbit

$$\bar{q}(t) = \bar{q}_0 \cos \omega t \tag{27}$$

with $\bar{q}_0 = a_3$ as defined by the multiple time scales method. The related $\bar{x} = \bar{z}_1$ and $\bar{y} = \bar{z}_2$ target variables are therefore

$$\bar{z}_i = \frac{\varepsilon\alpha_i\bar{q}_0^2}{4} + \sum_{k=1}^{2} \frac{\varepsilon\alpha_i\omega_i^2(\bar{q}_0/k)^k}{\sqrt{(\omega_i^2 - (k\omega)^2)^2 + (k\varepsilon\lambda_i\omega)^2}} \cos\left[k\omega t - \arctan\left(\frac{k\varepsilon\lambda_i\omega}{\omega_i^2 - (k\omega)^2}\right)\right]$$

$$= \sum_{k=0}^{2} A_{ik}\cos(k\omega t - \phi_{ik}). \tag{28}$$

The second equality explicitly defines the A_{ik} and ϕ_{ik} coefficients.

The stability of the feedback controller depends on the value of the scalar feedback parameter K. It is very important to stress that stability corresponds to the boundedness condition

$$\lim_{t\to+\infty} \|\mathbf{u}(t) - \bar{\mathbf{u}}(t)\| < +\infty \tag{29}$$

which is quite different from the control condition (25). Therefore, the stability of the feedback controller does not necessarily correspond to the achievement of a satisfying control.

A common approach to check for the stability of the controller is the determination of the instantaneous eigenvalues of the associated Jacobian on the target orbit, that is

$$\mathbf{J}^{(\mathbf{c})} = \left[\frac{\partial \mathbf{F}_\mathbf{i}^{(\mathbf{c})}}{\partial \mathbf{u}_\mathbf{j}}\right]_{\mathbf{u}=\bar{\mathbf{u}}}. \tag{30}$$

The controlled transducer will be considered as stable if all these eigenvalues are uniformly negative. Applying the Routh–Hurwitz criterion on the resulting characteristic sixth order polynomial yields the following stability condition:

$$K > -1 - 3\gamma_0\bar{q}^2 + (\mu_1\bar{x} + \mu_2\bar{y}) + \beta_{12}(1+\bar{q})^2. \tag{31}$$

In fact, the stability of the control process rigorously depends on the asymptotic behaviour of the deviation variable

$$p(t) = q(t) - \bar{q}(t) \tag{32}$$

which is the measure of the relative nearness between the controlled and the target orbits. At a linear approximation, p obeys to

$$\ddot{p} + \varepsilon\lambda_e\dot{p} + \bar{Q}(t)p = \bar{R}(t), \tag{33}$$

where the residue function $\bar{R}(t)$ can approximately be expressed as

$$\bar{R}(t) = \sum_{k=1}^{2} \varepsilon\mu_k\left[\left(A_{k0} + \tfrac{1}{2}A_{k1}\bar{q}_0\right) + \left(A_{k2} + \tfrac{1}{2}A_{k1}\bar{q}_0\right)\cos 2\omega t\right]$$

$$+ \left[-\tfrac{1}{4}\varepsilon\gamma\bar{q}_0^3 + \sum_{k=1}^{2}\tfrac{1}{2}\varepsilon\mu_k A_{k2}\bar{q}_0\right]\cos 3\omega t$$

$$= \sum_{k=0}^{3} \bar{R}_k\cos(k\omega t) \tag{34}$$

while the multiperiodic function $\bar{Q}(t)$ reads

$$\bar{Q}(t) = 1 + K + \tfrac{3}{2}\varepsilon\gamma\bar{q}_0^2(1+\cos 2\omega t) - \sum_{i=1}^{2}\sum_{k=0}^{2}\varepsilon\mu_i A_{ik}\cos(k\omega t)$$

$$= \sum_{k=0}^{2}\bar{Q}_k\cos(k\omega t). \tag{35}$$

As for Eq. (28), the second equalities in Eqs. (34) and (35) define the $\bar{R}_k$ and $\bar{Q}_k$ coefficients. The phase shifts have been discarded to exacerbate resonance and lead to the most constraining stability requirements. It should be noticed that $\bar{R}_1 \equiv 0$ because the target orbit which has been chosen is supposed to be the best uniperiodic approximation of the UPOs of the chaotic attractor. On the other hand, the variation of the feedback control parameter K will exclusively influence the coefficient $\bar{Q}_0$.

The stability problem is now associated to Eq. (33) which is a damped Floquet equation with multi-frequency external and parametric excitation. The analytic treatment of such equations is quite complicated, but however, depending to the various parameters (and mainly K as far as it is of concern), the parametric resonance induced by $\bar{Q}(t)$ can provoke an unbounded growth to infinity for p, i.e., for the electric charge q [1,15,16]. When the competition between the different frequencies of $\bar{Q}(t)$ is weak, the analytic determination of the stability boundaries can be performed [15]. The corresponding stability pattern is in the most general case constituted of a finite alternate sequence of instability and stability intervals for K. More precisely, the first of them is a semi-infinite unstable interval of the kind $]-\infty, K_a[$, while the last of them is a semi-infinite stable interval of the kind $]K_b, +\infty[$, K_a and K_b being boundary values. Between K_a and K_b, compact stable and unstable intervals are intermingled. It should be noticed that the straightforward eigenvalue approach cannot enable to recover this complex stability pattern, since the controller stability condition (31) is only equivalent to the constraint $\bar{Q}(t) > 0$, i.e., to the trivial requirement of a uniformly positive time-dependent stiffness function for p.

4.2. Threshold feedback control value

The unstable intervals are obviously dangerous for the electromechanical system, and should be avoided in priority. In practice, K is preferably chosen within the last and semi-infinite stable interval. Nevertheless, for a given required precision h, there is a critical value K_{cr} in that interval under which a convenient control is impossible. An estimation of this threshold feedback control value is of extreme importance since it would enable one to achieve the process with approximately the minimum input energy.

If the tolerated control error $h_q = max(|p(t)|)$ is small enough, the convenient K values are so high that both $\bar{Q}_1$ and $\bar{Q}_2$ become negligible relatively to $\bar{Q}_0$. Therefore, $p(t)$ will be a multiperiodic oscillation of maximal amplitude

$$p_{max} = \bar{R}_0 + \sum_{k=1}^{3}\frac{|\bar{R}_k|}{\sqrt{(\bar{Q}_0 - (k\omega)^2)^2 + (k\varepsilon\lambda_e\omega)^2}}. \tag{36}$$

Note that the phase shifts are still discarded. The threshold feedback control parameter is precisely obtained by setting $p_{max} = h_q$, so that K_{cr} may explicitly be expressed in first approximation as

$$K_{cr} = -1 - \tfrac{3}{2}\varepsilon\gamma\bar{q}_0^2 + \sum_{k=1}^{2} \varepsilon\mu_k A_{k0} + \tfrac{1}{2}\Phi\left[1 + \sqrt{1 - \frac{4\Psi}{\Phi^2}}\right], \tag{37}$$

where

$$\Phi = 13\omega^2 + \frac{|\bar{R}_2| + |\bar{R}_3|}{h_q - \bar{R}_0},$$
$$\Psi = 36\omega^4 + \frac{9|\bar{R}_2| + 4|\bar{R}_3|}{h_q - \bar{R}_0}\omega^2. \tag{38}$$

Hence, the control is supposed to succeed for $K > K_{cr}$, and to fail otherwise. It is important to stress that the analytic expression of K_{cr} in Eq. (37) can only be considered as an interesting quantitative estimation and an order of magnitude indicator, since the $\bar{R}_k$ and $\bar{Q}_k$ coefficients have been approximated. However, Eq. (37) indicates that K_{cr} is greater when the amplitude of the target orbit is high and the control error small. In Fig. 6, the numerical simulation of the controlled equations of motion has enabled the determination of K_{cr} for a given range of h_q values. One can notice the monotonous decrease of K_{cr} as h_q is increased. When the control condition $K > K_{cr}$ is fulfilled, the chaotic oscillations are progressively tuned to the desired optimal orbit, as it can be seen in Fig. 7.

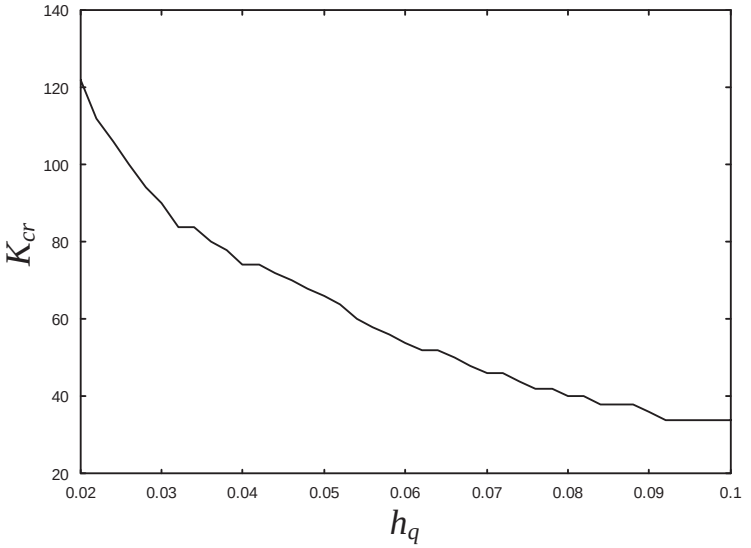

Fig. 6. Variations of K_{cr} as a function of h_q. Same parameters as for Fig. 5 with $U_0 = 10.0$, $\xi = -0.1$ and $\bar{q}_0 = 1.17623$.

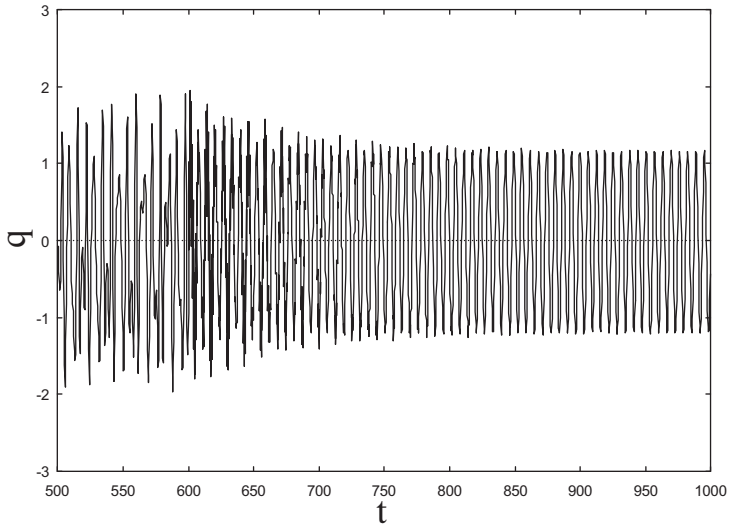

Fig. 7. Controlling the chaotic oscillations to the target orbit, with $K = 100$. The parameters are as for Fig. 6, and the control begins at the time $T_0 = 600$.

5. Conclusion

In this paper, we have studied the dynamics of a non-linear electrostatic transducer with two outputs has been studied, both in the regular and chaotic regimes. The equilibrium states have been determined, and their related stability has been studied. The investigations have led to the analysis of the TRS corresponding to the states of maximal exchange energy. The frequency response amplitudes and their stability have been analyzed. The conventional engineering approach of automatic control has been used to tune the chaotic oscillations to optimized regular target orbits. The stability analysis of the feedback controller has been performed, and critical values for the feedback control parameter have been derived.

Extensions for such a study are numerous. To name just a few, the analysis of the non-linear transducer under multi-frequency or stochastic external excitation, the study of other types of electromechanical systems and electroacoustic transducers, or the synchronization of several such devices would certainly be of great practical and theoretical interest.

References

[1] A.H. Nayfeh, D.T. Mook, *Nonlinear Oscillations*, Wiley, New York, 1979.
[2] J. Awrejcewicz, *Bifurcation and Chaos in Coupled Oscillators*, World Scientific, Singapore, 1991.
[3] E. Mosekilde, L. Mosekilde, *Complexity, Chaos and Biological Evolution*, Nato ASI Series B: Physics, Vol. 270, Plenum Press, New York, 1992.
[4] P. Woafo, J.C. Chedjou, H.B. Fotsin, Dynamics of a system consisting of a Van der Pol oscillator coupled to a Duffing oscillator, *Physical Review E* 54 (1996) 5929–5934.

[5] H.F. El-Bassiouny, M. Eïssa, Response of three-degree-of-freedom system with cubic nonlinearities to harmonic excitations, *Physica Scripta* 59 (1999) 183–194.
[6] J.K. Cheng, K.W. Wang, Stability and nonlinear dynamics of a horizontal base-excited rigid rod with unsymmetric end stiffnesses, *Journal of Vibration and Acoustics* 115 (1993) 85–95.
[7] J.C. Chedjou, P. Woafo, S. Domngang, Shilnikov chaos and dynamics of a self-sustained electromechanical transducer, *Journal of Vibration and Acoustics* 123 (2001) 170–174.
[8] P. Woafo, H.B. Fotsin, J.C. Chedjou, Dynamics of two nonlinearly coupled oscillators, *Physica Scripta* 57 (1998) 195–200.
[9] Y. Chembo Kouomou, P. Woafo, Stability and chaos control in electrostatic transducers, *Physica Scripta* 62 (2000) 255–260.
[10] J.C. Chedjou, H.B. Fotsin, P. Woafo, S. Domngang, Analog simulation of the dynamics of a Van der Pol oscillator coupled to a Duffing oscillator, *IEEE Transactions on Circuits and Systems I* 48 (2001) 748–757.
[11] P. Woafo, Transitions to chaos and synchronization in a nonlinear emitter–receiver system, *Physics Letters A* 267 (2000) 31–39.
[12] G. Chen, X. Dong, On feedback control of chaotic continuous-time systems, *IEEE Transactions on Circuits and Systems I* 40 (1993) 591–601.
[13] T. Kapitaniak, *Controlling Chaos*, Academic Press, London, 1996.
[14] M. Lakshamanan, K. Murali, *Chaos in Non-linear Oscillators, Controlling and Synchronization*, World Scientific, Singapore, 1996.
[15] Y. Chembo Kouomou, P. Woafo, Stability and optimal parameters for continuous feedback chaos control, *Physical Review E* 66 (2002) 036205.
[16] C. Hayashi, *Nonlinear Oscillations in Physical Systems*, McGraw-Hill, New York, 1964.